General Assembly, Vienna , Austria 7-12 April 2019

UNIL | Université de Lausanne
Institut des sciences de la Terre

FONDS NATIONAL SUISSE
SCHWEIZERISCHER NATIONALFONDS
FONDO NAZIONALE SVIZZERO
SWISS NATIONAL SCIENCE FOUNDATION

This presentation participates in OSPP
Outstanding Student Poster & PICO Contest
Poster N. 7129

Constructing a crustal 3-D shear-wave velocity model based on converted waves: from Forward Model to Inversion

Contact: leonardo.colavitti@unil.ch
Group website: http://wp.unil.ch/orog3ny
AlpArray website: http://www.alparray.ethz.ch

Leonardo Colavitti [(1)], **György Hetényi** [(1)] **& AlpArray Working Group**

[(1)] **Institute of Earth Sciences, University of Lausanne, Lausanne, Switzerland**

MOTIVATION

We develop a new tool where P-to-S converted waves are exploited in order to construct a fully 3-D shear-wave velocity model of the crust.
Our approach is deeply different from ANT and LET, as it uses sub-vertical rays.
This method is based on receiver functions (RFs) and requires a dense seismological network to investigate the less-studied S-wave velocities (Christensen, 1996).

DATASET AND METHOD

For the benchmark study we focus on the Central Alps, using both permanent and AlpArray stations (Hetényi et al., 2018) in order to get a homogeneous coverage of our zone (**Figure 1**).
Our dataset is composed of the last 20 years' of high-quality data (**Figure 2**).

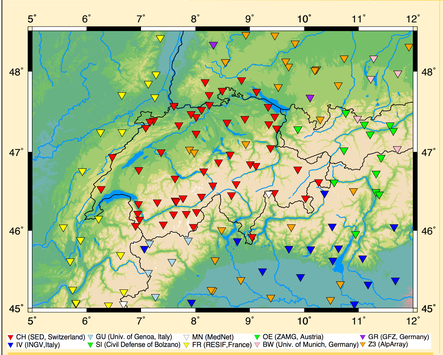

Figure 1 Seismic stations available in the Central Alps.

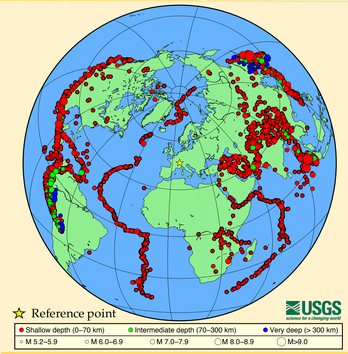

Figure 2 Earthquakes used for receiver functions.

We compute RFs to map Earth discontinuities at depth.
The difference in travel time between the converted S-wave and direct P-wave contains information about the depth to the boundary and velocity relations.

N. Stations:	150
N. Events:	6450
Ep. Distance:	25° – 95°
Magnitude:	≥ 5.2
Frequency:	0.125-0.5 Hz
Deconvolution	Ligorría and
Algorithm:	Ammon (1999)

MODEL PARAMETERIZATION

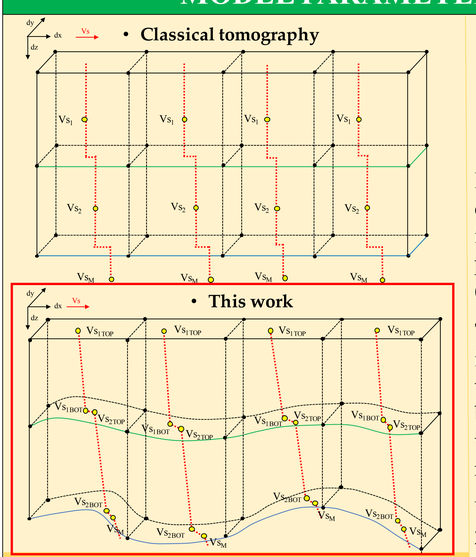

Figure 3 Comparison between model discretization in classical tomography and the parameterization used in this work.

Legend
- Mesh node
- Velocity value is defined
- Interface 1
- Interface 2
- Velocity profile

In this work we consider that a discontinuity is laterally variable in depth and also that the velocity profile per layer can be a gradient (**Figure 3**).

The introduction of this flexibility in the discontinuity (given by 2 velocity for each node, above and below) allows us to investigate the velocity jump between neighbouring layers.

We first plan to create and test a 2-layer Vs model for the Alpine region.

RAY TRACING IMPLEMENTATION IN 3D

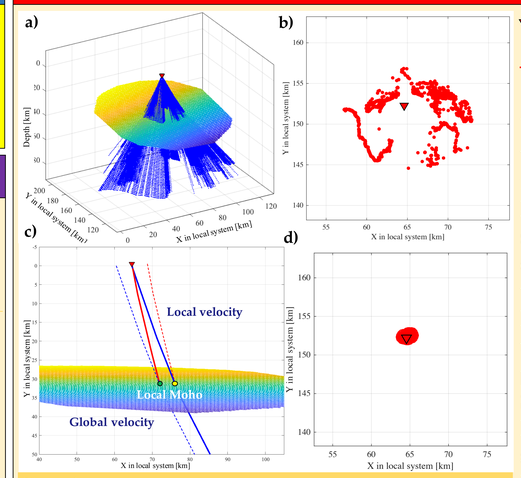

Figure 4
a) P-wave raypath in a global velocity model.
b) S-wave arrival points to the station at the surface before correction.
c) Example of a correct shooting.
d) S-wave arrival to the station after 2nd shooting.

▼ Position of stations
P-wave raypath [p1] — P-wave raypath [p2]
S-wave raypath [s1] — S-wave raypath [s2]
Piercing point at local Moho [s1] • Piercing point at local Moho [s2]

We implement an accurate ray-propagator which respects Snell's law in 3-D at any interface geometry.
First (**Fig. 4a**), we employ an existing ray shooting tool (Knapmeyer, 2004) to calculate P-ray geometry in a global velocity model iasp91 (Kennet and Engdahl, 1991), so the P-wave arrives at the station. Then, starting from the piercing point at the local Moho, we shoot an S-wave (**Fig. 4b**).
During wave conversion, we take into account the true Moho dip **(Fig. 4c** and **5)**. Finally we adjust the ray parameter to make the S-waves arrive at the station (**Fig.4d**).

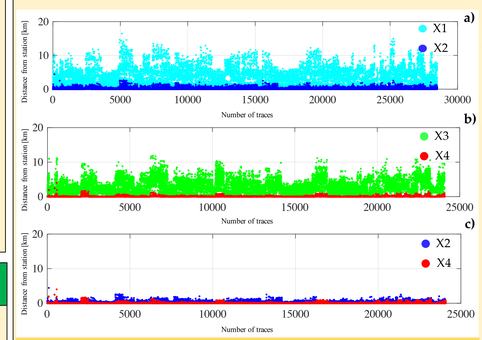

Figure 6
a) 1st and 2nd shooting using Diehl's velocity model as input.
b) 1st and 2nd shooting using our initial velocity model as input.
c) Final shootings considering Diehl and our initial velocity model.

Phase	Numb. RFs
Initial Data	287 414
QC on Z-N-E	116 804
QC on RFs	28 494
Ray Trace 1	24 148
Ray Trace 2	24 084

Table 1
RFs active traces during different procedures.

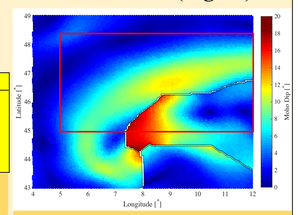

Figure 5 Moho dip map.

As shown in **Figure 6**, after 2nd shooting, considering a local 3-D velocity structure (Diehl et al., 2009) and a complex Moho geometry (Spada et al., 2013), the mean distance between the arriving S-wave and the station is 190 m (median ~60 m).
This distance decreases to 75 m (median ~30 m), when considering our initial velocity model.

COVERAGE AND MISFIT MAPS

For each trace, we compute a misfit using L2-norm. **Figure 8** shows the misfit at the Moho depth for each trace.
In **Figure 9** we represent the same misfit, considering the crustal path from Moho to station. Moreover, we add the Fresnel zone with f_{max} = 0.5 Hz and V_s = 4.47 km/s.

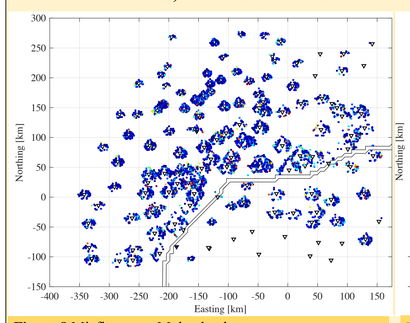

Figure 8 Misfit map at Moho depth.
Black lines represent the plate boundary between Adria and Europe.

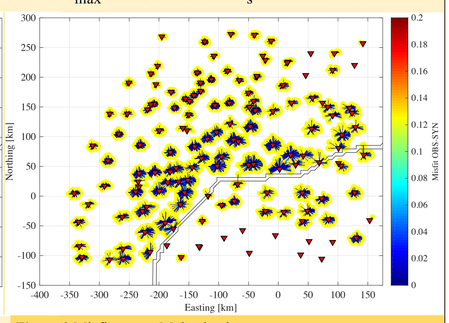

Figure 9 Misfit map at Moho depth.
Lines represent the raypath from the Moho to the station.
Yellow areas show the Fresnel zone at the Moho depth.

Figure 10 shows the ray coverage map for the case where cells are 25x25 km in X-Y.
Combining the information on the nodes of our parameterization and the distribution of piercing points, we can compute at each node a misfit using a weighted mean (**Fig. 11**).
To avoid gaps in the central area, we apply an overlap between neighbouring averaging zones.

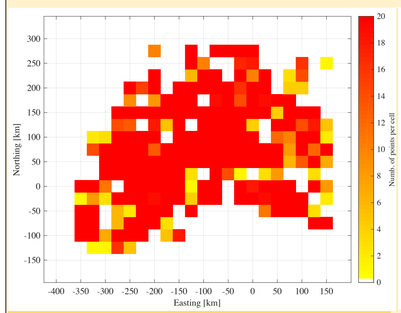

Figure 10 Coverage Map of our area at Moho depth.
Red cells shows are crossed by at least 20 points (up to 829).

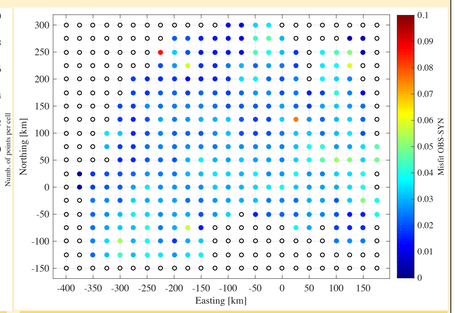

Figure 11 Misfit map at Moho depth, considering nodes of our area.
Misfit values are computed using linear weighted mean and overlap.

OBSERVED – SYNTHETIC RFs COMPARISON

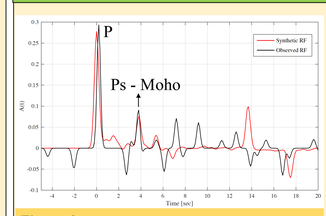

Figure 6
Comparison between observed and synthetic RF for the Chiapas earthquake, Mexico (2017-09-08, 04:49:19 UTC) at the station ZUR.

For each observed trace, synthetic RFs (Shibutani et al., 1996) are obtained using 1-D velocity models (**Fig. 6**) which are extracted from the 3-D structure along rays.
The velocity at each step is computed by a weighted mean of velocities at the enclosing mesh nodes (**Fig. 7**).

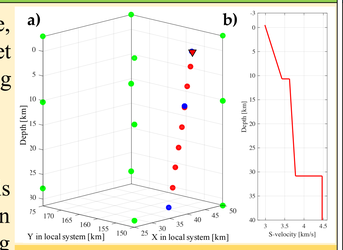

Figure 7 a) Representation of raypath in 3-D.
b) 1-D Vs model for synthetic RF calculation.

INVERSION APPROACH

We envisage to guide the inversion using an iterative method based on conjugate gradients, as we have a large, sparse matrix.
The model perturbation is carried out node by node, and only the affected RFs have to be computed until a local minimum is reached. Then all subsequent nodes are perturbed along a path to be defined over the zone covered by rays.

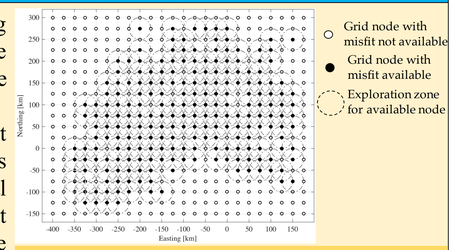

Figure 12 Iterative inversion approach. The search for nodes with ray coverage (black dots) allows us to reduce the computation time.

REFERENCES

- Christensen, N. I., 1996. *J. Geophys. Res.*, **101 (B2)**, 3139-3156.
- Diehl, T. et al., 2009. *Geophys. J. Int.*, **179**, 1133-1147.
- Hetényi, G. et al., 2018. *Surv. Geophys.* **39**, 1009-1033.
- Kennett, B. L. N. and Engdahl, E. R., 1991. *Geophys. J. Int.* **105,** 429-465.
- Knapmeyer, M., 2004. *Seismol. Res. Lett.*, **75(6)**, 723-726.
- Ligorría, J. and Ammon, C. J., 1999. *B. Seismol. Soc. Am.* **89(5)**, 1395-1400.
- Shibutani, T. et al., 1996. *Geophys. Res. Lett.* **23(14)**, 1829-1832.
- Spada, M. et al. 2013. *Geophys. J. Int.*, **194(2)**, 1050-1068.

ACKNOWLEDGEMENTS

We are very grateful to the Swiss Seismological Service, Istituto Nazionale di Geofisica e Vulcanologia in Italy, University of Genova, Civil Defense of Bolzano, Mediterranean Network, Réseau simologique et géodésique français, Zentralanstalt für Meteorologie und Geodynamic in Austria, University of Münich, German Research Centre for Geosciences and AlpArray project for collecting and sharing seismological data.
We also say thanks to Prof. N. Linde (Institute of Earth Sciences in Lausanne, Switzerland), Dr. T. Bodin (Laboratoire de Géologie de Lyon, France) and the researchers of AlpArray RF Working Group for their fruitful advice during this research and Dr. T. Diehl (Swiss Seimological Service, Zürich, Switzerland for making the 3-D P-velocity model of the Alps available.
This research is supported by the Swiss National Science Foundation grant number PP00P2_157627.